https://doi.org/10.1016/j.advengsoft.2017.12.003

Advances in Engineering Software

Noise attenuation capacity of a Helmholtz resonator

Chenzhi Cai and Cheuk Ming Mak *

Department of Building Services Engineering, The Hong Kong Polytechnic University,

Hung Hom, Kowloon, Hong Kong, China

chenzhi.cai@connect.polyu.hk, cheuk-ming.mak@polyu.edu.hk

*Corresponding author.
E-mail Address: cheuk-ming.mak@polyu.edu.hk (C.M.Mak).
Telephone: +852 2766 5856
Fax: +852 2765 7198

Abstract

Helmholtz resonator (HR) is one of the most basic acoustic models and has been widely used in engineering applications due to its simple, tunable and durable characteristics. The transmission loss index is mainly used to evaluate the acoustic transmission performance. Based on the transmission loss index, this paper proposes the noise attenuation capacity index as one of the key parameters to evaluate the noise attenuation performance of a HR. The noise attenuation capacity is defined as the integral of transmission loss in the frequency domain. The theoretical formula of a HR's noise attenuation capacity is first derived in this study. It indicates that the noise attenuation capacity of a HR is only related to geometries of the neck and duct's cross-sectional area. The cavity volume has no effects on its noise attenuation capacity. The proposed theoretical formula of a HR's noise attenuation capacity is validated by Finite Element Method (FEM) simulation using commercial software (COMSOL Multiphysics). The proposed noise attenuation capacity of a HR should therefore be considered as one of the main acoustic characteristics of a HR. It is hoped that the present study could provide a stepping stone for the investigation of the HR's or other silencers' noise attenuation capacity and potential applications in all research areas in respect of the HR.

Keywords: Helmholtz resonator; transmission loss; noise attenuation capacity; finite element method

1. Introduction

The Helmholtz resonator (HR), which consists of a cavity communicating with an external duct through an orifice, is a well-known device to reduce noise centralized in a narrow band at its resonance frequency. Owing to the resonance frequency of a HR is only determined by its geometries, it is therefore straightforward to obtain a HR with a desired resonance frequency [1,2]. It is because of its simple, tunable and durable characteristics, the HR has been utilized in numerous duct-structure systems, such as ventilation and air conditioning system in buildings, automotive duct systems and aero-engines, for the attenuation of noise produced by unavoidable in-ducted elements [3,4]. Moreover, the applications of HRs extend to other research areas, for instance notch filters [5] and ultrasonic metamaterials [6].

Since the widespread applications of the HR, it has received a great deal of attentions worldwide. A lot of achievements have been made and are documented in numerous pieces of literature. Many studies have tried to obtain an accurate prediction of the resonance frequency. Initially, the HR is regarded as an equivalent spring-mass system. The mass of air in the neck is driven by an external force and the air inside the cavity acts as a spring [7]. Furthermore, wave propagation in both the neck and cavity has been considered in theoretical analysis. The wave propagation approach has developed from a one-dimensional approach in preliminary investigations to a multidimensional approach for the sake of accuracy [8,9]. Because of the HR is one of the most basic acoustics models as well as the narrow-band behavior at its resonance frequency, a wealth of literature also exists on the modification forms of HRs in order to improve the acoustic performance of a HR. The effects of different orifices and cavity geometries on the acoustics performance have

been studied [10]. Besides, some novel HRs have been proposed and investigated, for instance HR with extended neck or spiral neck [11], dual HR [12], coupled HR [13,14], HR with a coiled air cavity [15] and micro-perforated panel absorbers backed by HR (MPPHR) [16]. The major concerns of these modification forms of HRs are related to the transmission loss performance in the frequency domain.

The transmission loss index is indeed a major index and has been widely used to assess the acoustic transmission performance in the frequency domain. However, almost all researches concentrate on the shapes of the transmission loss curve while ignoring the area under the transmission loss curve. The noise attenuation capacity index defined as the integral of transmission loss in the frequency domain is therefore proposed to be one of the key parameters to evaluate HR's noise attenuation performance. The theoretical formula of a HR's noise attenuation capacity is first derived in this paper. Then, the three-dimensional Finite Element Method simulation using commercial software (COMSOL Multiphysics) is adopted to verify the correctness of the proposed theoretical formula. The proposed noise attenuation capacity should be considered as one of the main acoustic characteristics of a HR. It hopes that the present study could provide a stepping stone for the investigation of the HR's or other silencers' noise attenuation capacity and potential applications in all research areas in respect of the HR.

2. Theoretical analysis of the noise attenuation capacity of a Helmholtz resonator

The sudden discontinuous areas, for instance the duct-neck interface and the neck-cavity interface, result in a clearly multidimensional sound fields inside a HR [18]. Although a multidimensional approach could provide a more accurate prediction of the acoustic impedance of a HR, the main purpose here is to reveal the HR's noise attenuation

capacity. Moreover, the dimensions of the traditional HRs are significant small compared to the wavelengths of the concerned low frequencies in this study. It is therefore that classical equivalent spring-mass system is adopted here by introducing an end correction factor to account for the effects of evanescent high-order modes.

2.1 The classical lumped approach of a Helmholtz resonator

For the sake of completeness, a brief review of the classical lumped approach of a HR is appropriate here. A mechanical analogy of a single HR is illustrated in Fig. 1. The mass of air in the neck $M_m = \rho_0 S_n l_n'$ is driven by an external time-harmonic sound pressure force $F = S_n p_0 e^{j\omega t}$ and the cavity is regarded as a massless spring with stiffness $K_m = \rho_0 c_0^2 S_n^{\ 2} / V_c$ (where p_0 is the oscillation sound pressure, ρ_0 is air density, c_0 is the speed of sound in the air , l_n' and S_n are the neck's effective length and area respectively, ω is the angular frequency, and V_c is the cavity volume). The damping coefficient R_m of a HR is mainly caused by viscous dissipation through the neck, which is determined by acoustic screen across the area of the neck. By applying the Newton's second law of motion to the one degree of freedom HR, the oscillatory differential equation can be expressed as [1]:

$$M_m \frac{d^2 x}{dt^2} + R_m \frac{dx}{dt} + K_m x = S_n p_0 e^{j\omega t} \tag{1}$$

where x is the displacement of the mass, $v = dx/dt$ represents the velocity of the mass.

Owing to the different concerns between an acoustic system and a mechanical system, Eq. (1) should be rewritten in the form of volume velocity $U = vS_n$ as:

$$M_a \frac{dU}{dt} + R_a U + C_a \int U dt = p_0 e^{j\omega t} \tag{2}$$

where $M_a = M_m / S_n^2$, $R_a = R_m / S_n^2$ and $C_a = S_n^2 / K_m$ represent the sound mass, sound resistance and sound capacitance respectively in analogy of a circuit. The impedance of the HR can be derived from the solution of Eq. (2) as:

$$Z_r = \frac{p}{U} = R_a + j(\omega M_a - \frac{1}{\omega C_a}) \tag{3}$$

It is therefore that the resonance frequency of the HR can be derived from Eq. (3) and be expressed as $f = \sqrt{1/M_a C_a}\,/2\pi = c_0\sqrt{S_n / l_n' V_c}\,/2\pi$. Once the impedance is obtained, the transmission loss of a side-branch HR mounted on a duct with cross-sectional area S_d can be expressed as:

$$TL = 20\log_{10}(\frac{1}{2}\left|2 + \frac{\rho_0 c_0}{S_d}\frac{1}{Z_r}\right|) \tag{4}$$

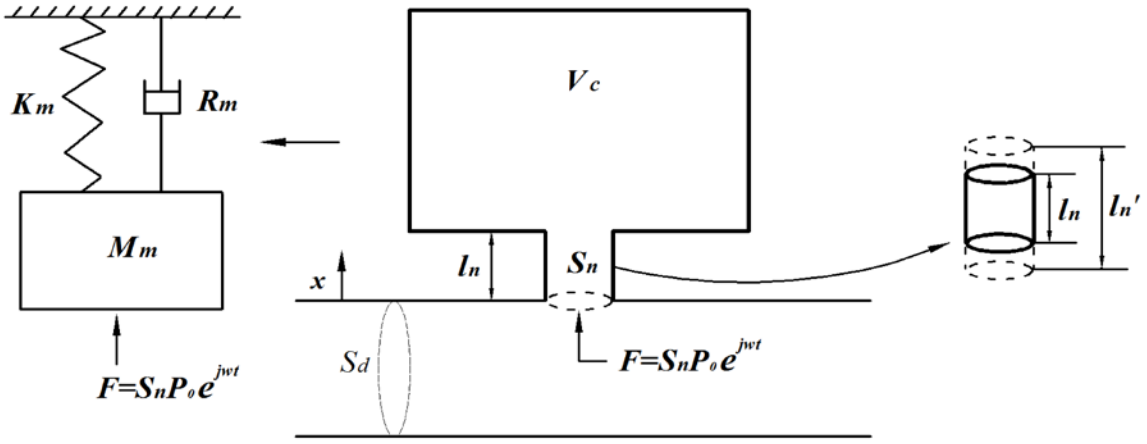

Fig.1 Mechanical analogy of a Helmholtz resonator

2.2 Noise attenuation capacity of a Helmholtz resonator

The transmission loss index is mainly used to evaluate the acoustic transmission performance in the frequency domain. However, it cannot provide a quantitative characteristic of the noise attenuation band. It is therefore that this paper proposes the noise

attenuation capacity index as one of the key parameters to evaluate the HR's noise attenuation performance quantitatively and distinctly. The noise attenuation capacity C_{TL} which is defined as the integral of transmission loss in the frequency domain, could be expressed as:

$$C_{TL} = \int TL df = \frac{1}{2\pi}\int TL d\omega = \frac{1}{2\pi}\int 20\log_{10}\left(\frac{1}{2}\left|2+\frac{\rho_0 c_0}{S_d}\frac{1}{Z_r}\right|\right)d\omega \tag{5}$$

The effect of viscous dissipation through the neck is ignored for simplicity. It is therefore that R_a in Eq. (3) equals zero. Then, substituting Eq. (3) into Eq. (5) gives:

$$\int TL d\omega = \int 10\log_{10}\left((B\omega^2 - C)^2 + A^2\omega^2\right)d\omega - \int 10\log_{10}(B\omega^2 - C)^2 d\omega \tag{6}$$

where $A = \rho_0 c_0 / 2S_d$, $B = \rho_0 l_n' / S_n$ and $C = \rho_0 {c_0}^2 / V_c$ are constants related to geometries of the HR and the duct. The antiderivative of the first term on the right-hand side of Eq. (6) can be solved as:

$$\begin{aligned}&\int 10\log_{10}\left((B\omega^2 - C)^2 + A^2\omega^2\right)d\omega = \int 10\log_{10}\left(B^2(\omega^2+a)(\omega^2+b)\right)d\omega \\ &= \int 10\log_{10}B^2 d\omega + \int 10\log_{10}(\omega^2+a)d\omega + \int 10\log_{10}(\omega^2+b)d\omega\end{aligned} \tag{7}$$

and

$$\begin{cases} \int 10\log_{10}B^2 d\omega = 20\omega\log_{10}B \\ \int 10\log_{10}\left((\omega^2+a)\right)d\omega = 10\left[\dfrac{\omega\ln(\omega^2+a)}{\ln 10} - \dfrac{2[\omega - \sqrt{a}\arctan(\omega/\sqrt{a})]}{\ln 10}\right] \\ \int 10\log_{10}\left((\omega^2+b)\right)d\omega = 10\left[\dfrac{\omega\ln(\omega^2+b)}{\ln 10} - \dfrac{2[\omega - \sqrt{b}\arctan(\omega/\sqrt{b})]}{\ln 10}\right] \end{cases} \tag{8}$$

where a and b should satisfy the requirements of $a+b = (A^2 - 2BC)/B^2$ and $ab = C^2/B^2$ simultaneously.

The antiderivative of the second term on the right-hand side of Eq. (6) can be derived as:

$$\int 10\log_{10}\left((B\omega^2-C)^2\right)d\omega=\int 10\log_{10}B^2d\omega+\int 10\log_{10}(\omega^2-c)^2d\omega$$

$$=20\omega\log_{10}B+10\left[\frac{\omega\ln(\omega^2-c)^2}{\ln 10}-\frac{4\omega-\sqrt{c}\left(\ln\left(\frac{\omega+\sqrt{c}}{\sqrt{c}}\right)^2-\ln\left(\frac{\omega-\sqrt{c}}{\sqrt{c}}\right)^2\right)}{\ln 10}\right] \quad (9)$$

Combining Eq. (7), Eq. (8) and Eq. (9), Eq. (6) can be rearranged as:

$$\int TLd\omega=\frac{10}{\ln 10}\left[\omega\ln\frac{(\omega^2+a)(\omega^2+b)}{(\omega^2-c)^2}+2\sqrt{a}\arctan(\omega/\sqrt{a})+2\sqrt{b}\arctan(\omega/\sqrt{b})-\sqrt{c}\ln\frac{(\omega+\sqrt{c})^2}{(\omega-\sqrt{c})^2}\right] \quad (10)$$

According to Eq. (10), the integral of transmission loss in the circular frequency domain can be calculated as:

$$\int_0^\infty TLd\omega=\frac{10\pi}{\ln 10}(\sqrt{a}+\sqrt{b})=\frac{10\pi}{\ln 10}\frac{A}{B}=\frac{5\pi}{\ln 10}\frac{c_0S_n}{S_dl_n'} \quad (11)$$

It should be noted that the quantities of a and b are not need to be solved to obtain the $\sqrt{a}+\sqrt{b}$. The quantity of $\sqrt{a}+\sqrt{b}$ can be obtained according to the relation of $(\sqrt{a}+\sqrt{b})^2=(a+b)+2\sqrt{ab}=(A/B)^2$ (where a and b should satisfy the requirements of $a+b=(A^2-2BC)/B^2$ and $ab=C^2/B^2$ simultaneously).

It is therefore that the noise attenuation capacity C_{TL} is derived as:

$$C_{TL}=\int_0^\infty TLdf=\frac{1}{2\pi}\int_0^\infty TLd\omega=\frac{5}{2\ln 10}\frac{c_0S_n}{S_dl_n'} \quad (12)$$

It can be seen from Eq. (12) that the noise attenuation capacity C_{TL} in the frequency domain is only related to the geometries of the neck and the cross-sectional area of the duct. The cavity volume has no effects on the HR's noise attenuation capacity. Similar to the

resonance frequency, Eq. (12) provides a distinct parameter to evaluate the HR's noise attenuation band quantitatively. Moreover, Eq. (12) indicates that the noise attenuation bandwidth and peak attenuation amplitude are complimentary to each other. There is no trick to noise control. It points out distinctly the impossibility for some struggles to obtain a broader noise attenuation band with higher peak amplitude for a determined side-branch HR system. The C_{TL} can therefore be considered as one of the main acoustic characteristics of a HR and be taken into consideration in noise control optimization and HR design.

3. Results and discussion

The three-dimensional FEM simulation using commercial software (COMSOL Multiphysics) is used to validate the correctness of the proposed theoretical formula of noise attenuation capacity. As low frequencies are the main concerns here, the frequency range considered here is well below the duct's cutoff frequency. Hence, only planar wave is assumed to propagate through the duct in all the FEM simulations. An oscillation sound pressure at a magnitude of $P_0 = 1$ Pa is applied at the beginning of the duct. An anechoic termination is applied at the end of the duct to avoid reflected waves.

3.1 Validation of the effects of cavity volume on HR's noise attenuation capacity

Three different HRs with fixed neck geometries $l_n = 4$ cm, $S_n = \pi$ cm^2 and three different cavity volumes $V_1 = 392.04\pi$ cm^3, $V_2 = 479.16\pi$ cm^3 and $V_3 = 653.4\pi$ cm^3 are used here, annotated as HR1, HR2 and HR3 respectively. The cross-sectional area of the main duct is set as $S_d = 36$ cm^2. The acoustic FEM models of these three side-branch HRs are built separately, as illustrated in Fig. 2. To ensure the accuracy, a fine mesh spacing of no more than 2.2 cm is maintained for these models. The mesh divides these three models more than 8000 triangular elements. The maximum element is observed in the duct with a

side length of around 2.2 cm; the minimum element can be observed in both the neck-duct interface and the neck-cavity interface with a side length of around 0.16 cm.

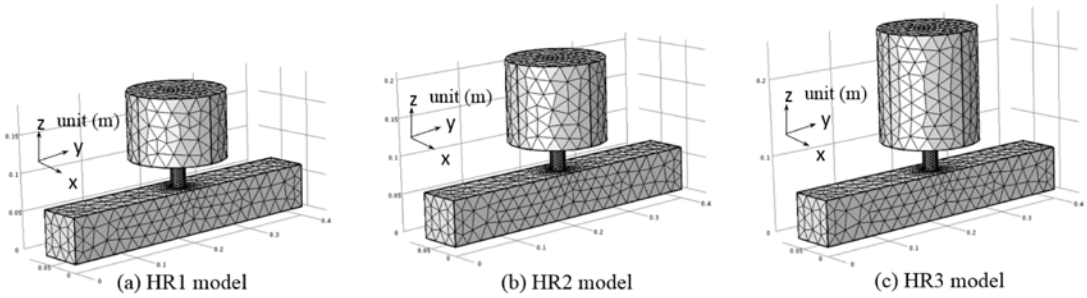

Fig. 2 The acoustic FEM models of side-branch HRs with respect to different HRs: (a) HR1 model, (b) HR2 model, (c) HR3 model

The comparison of theoretical predicted transmission loss and the FEM simulation results with respect to different HRs are illustrated in Fig. 3, and the predicted results are in good agreement with the FEM simulation results. It can also be observed that the resonance frequency of the HR decreased with the increasing cavity volume, as a well-known principle. However, the normalized predicted transmission losses of these three models are almost the same by normalizing to their corresponding resonance frequency, as demonstrated in Fig. 4. It indicates that the cavity volume has no effects on C_{TL}.

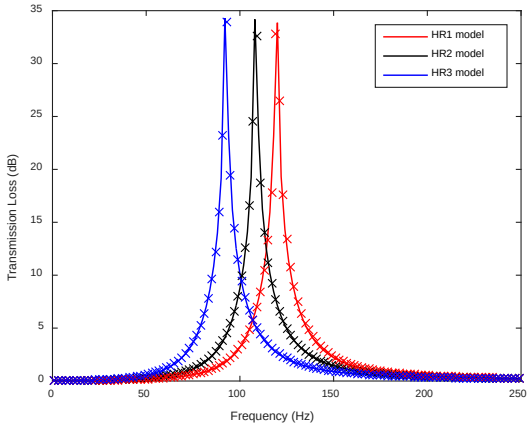

Fig. 3 Comparison of theoretical predictions and the FEM simulation results with respect to different HRs (solid lines represent the theoretical predictions, and dashed crosses represent the FEM simulation results)

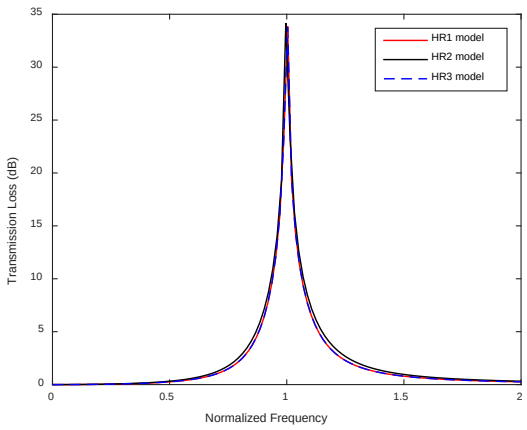

Fig. 4 Normalized transmission loss of different HRs

3.2 Validation of the effects of duct's cross-sectional area on HR's noise attenuation capacity

The geometries of the HR used here are the same as aforementioned HR2, which is mounted on the duct with different cross-sectional areas. The acoustic FEM models of the identical HR mounted on ducts in respect of different cross-sectional areas are demonstrated in Fig. 5, annotated as Sd1 model, Sd2 model and Sd3 model corresponding to different duct's cross-sectional areas $S_{d1} = 25$ cm^2, $S_{d2} = 36$ cm^2 and $S_{d3} = 64$ cm^2 respectively. Similar to aforementioned acoustic FEM models, a fine mesh system is conducted and it is not described in details here for simplicity. Fig. 6 compares the transmission loss of these models between the theoretical predictions and FEM simulation results. The theoretical predicted results agree well with the FEM simulation results. It can be observed that the resonance frequencies of these three models remain unchanged

due to the same HR used here. However, a much broader band with higher peak can be obtained through the decrease of the duct's cross-sectional area.

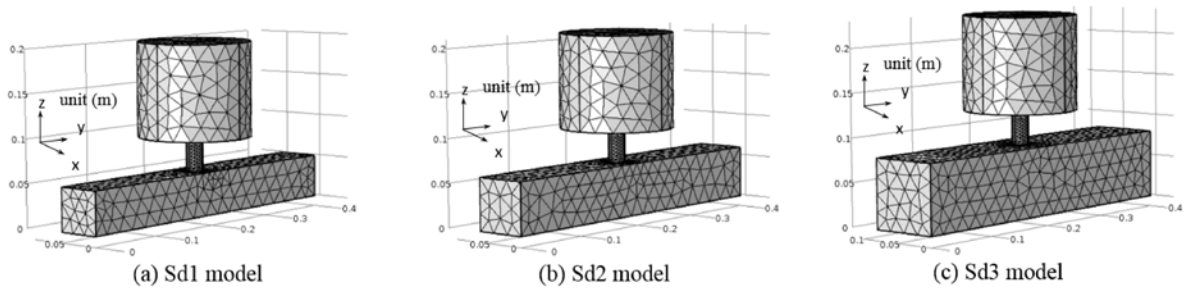

Fig. 5 The acoustic FEM models of the identical HR mounted on different ducts with respect to different cross-sectional areas: (a) Sd1 model, (b) Sd2 model, (c) Sd3 model

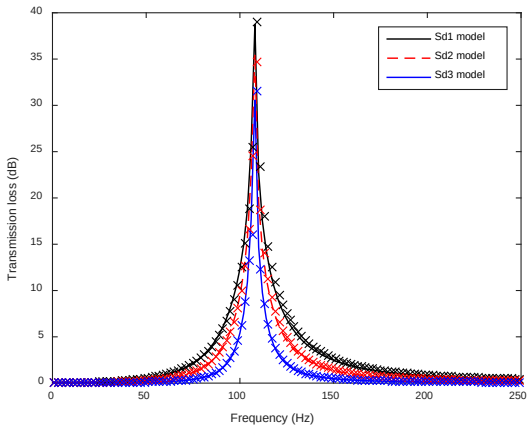

Fig. 6 The transmission loss of the identical HR mounted on ducts with different cross-sectional areas (solid lines represent the theoretical predictions, and dashed crosses represent the FEM simulation results)

3.3 Validation of the effects of neck's geometries on the HR's noise attenuation capacity

Six different HRs with fixed cavity volume $V = 479.16\pi$ cm^3 and different neck geometries are installed on the duct of cross-sectional area $S_d = 36$ cm^3 separately. The acoustic FEM models are exhibited in Fig. 7. The models annotated as ln1 model, ln2 model and ln3 model are corresponding to different necks with fixed cross-sectional area

$S_n = \pi$ cm^2 and different neck lengths $l_{n1} = 2$ cm, $l_{n2} = 4$ cm and $l_{n3} = 8$ cm respectively. The models annotated as Sn1 model, Sn2 model and Sn3 model are corresponding to necks with fixed length $l_n = 4$ cm and different cross-sectional areas $S_{n1} = 0.36\pi$ cm^2, $S_{n2} = \pi$ cm^2 and $S_{n3} = 2.25\pi$ cm^2 respectively. It should be noted that an identical model is named after two different names as ln2 model and Sn2 model in order for the convenience of investigations here.

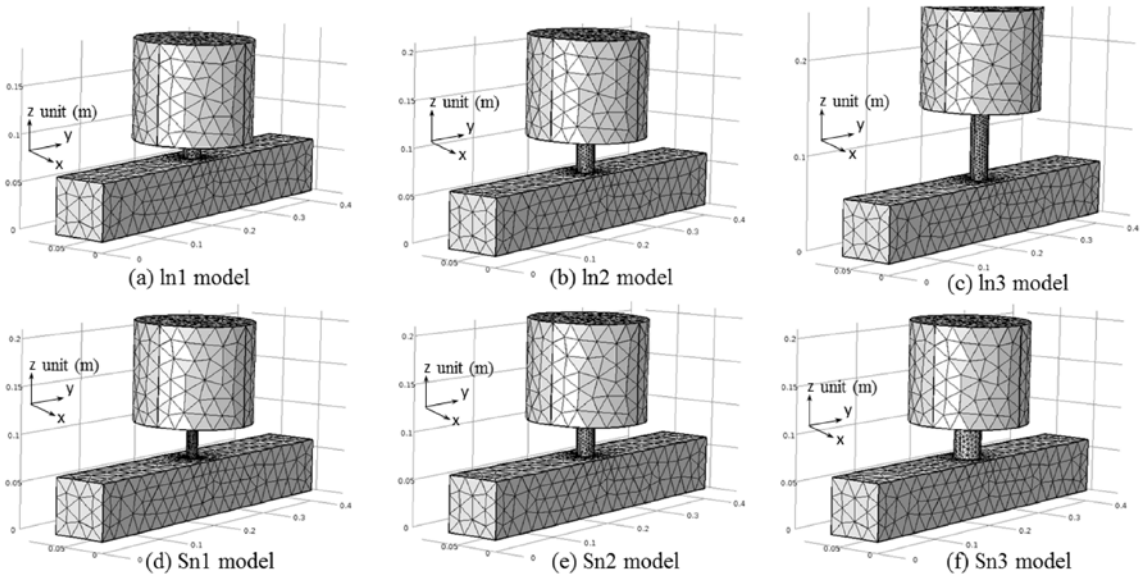

Fig. 7 The acoustic FEM models of side-branch HRs in respect of different neck geometries: (a) ln1 model, (b) ln2 model, (c) ln3 model, (d) Sn1 model, (e) Sn2 model, (f) Sn3 model

Fig. 8(a) compares the transmission loss between theoretical predictions and FEM simulation results with respect to different neck lengths. The comparison of theoretical predicted results and the FEM simulation results in respect of different cross-sectional areas of necks are demonstrated in Fig. 8(b). The predicted results fit well with FEM

simulation results in both Fig. 8(a) and Fig. 8(b). It can be observed in Fig. 8(a) that the increased neck length will decrease HR's resonance frequency as well as the bandwidth. Whereas, a broader bandwidth compromised with a higher resonance frequency can be obtained by increasing the cross-sectional area of the neck, as illustrated in Fig. 8(b). The changes in the resonance frequency of a HR is also a well-known principle. It is therefore that the concerns here focus on the noise attenuation bandwidth. The normalized predicted transmission losses of these models are demonstrated in Fig .9(a) and Fig. 9(b) corresponding to variations in neck length and neck's cross-sectional area respectively. A more obvious change of noise attenuation bandwidth due to the geometries of neck can be observed in Fig. 9.

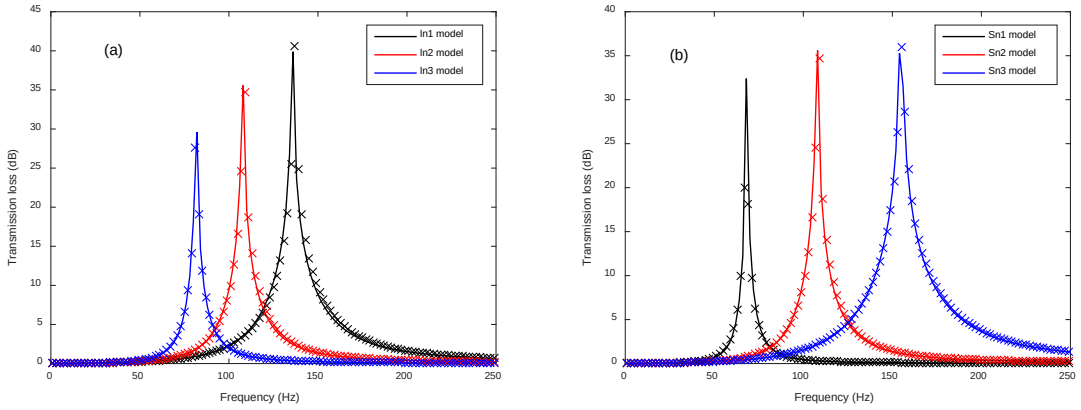

Fig. 8 Comparison of theoretical predictions and the FEM simulation results with respect to different HRs (solid lines represent the theoretical predictions, and dashed crosses represent the FEM simulation results)

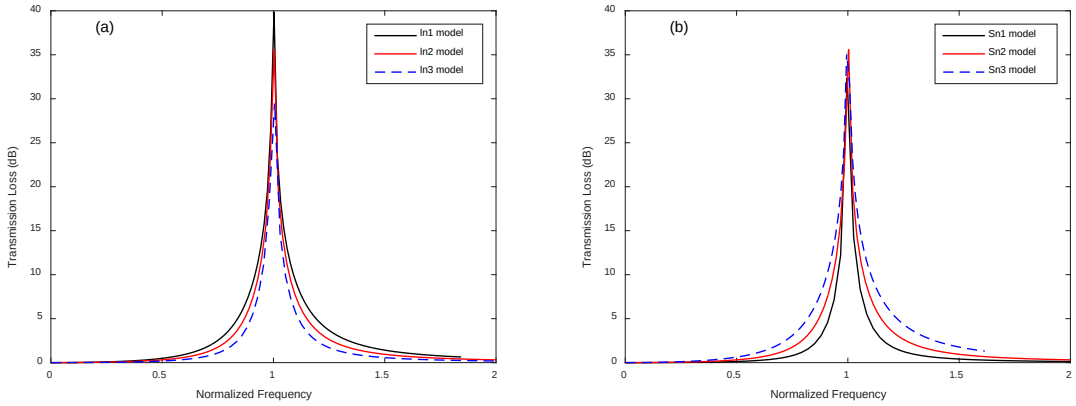

Fig. 9 Normalized transmission loss of different HRs

3.4 Validation of proposed equation for noise attenuation capacity

The aforementioned models imply the correctness of proposed Eq. (12). Furthermore, the noise attenuation capacity C_{TL} of those models above is exhibited in Table 1. It can be observed from Table 1 that the relative errors between the FEM simulation results and calculated values of Eq. (12) are less than 6%, 6.1% and 2.5% in the frequency ranges of 0~250 Hz, 0~350 Hz and 0~1000 Hz respectively. The transmission loss of ln1 model and Sn3 model do not approach zero at 250 Hz as demonstrated in Fig. 8. It is therefore that the chosen frequency range is 0~350 Hz rather than 0~250 Hz for the last six models. The results indicate that correctness of the C_{TL} calculated by Eq. (12) .The C_{TL} is only related to the geometries of the neck and the duct's cross-sectional area. The cavity volume of the HR has no effects on the C_{TL}. Similar to the significance of HR's resonance frequency, the proposed Eq. (12) for C_{TL} should therefore be considered as one of the main acoustic characteristics of a HR. It provides a distinct parameter to evaluate the HR's noise attenuation band quantitatively and illuminates the limitations in HR's noise control applications.

Table 1. Relative error between the FEM simulation result and value of Eq. (12)

		Models					
		HR1 model	HR2 model	HR3 model	Sd1 model	Sd2 model	Sd3 model
C_{TL}	FEM (0~250 Hz)	568.47	568.25	569.24	817.96	568.47	325.64
	Eq.(12)		603.58		869.15	603.58	339.51
	Relative error	5.8%	5.9 %	5.7%	5.9%	5.8%	4%
	FEM (0~1000 Hz)	589.76	590.2	589.69	848.17	590.2	331.52
	Eq.(12)		603.58		869.15	603.58	339.51
	Relative error	2.3%	2.2%	2.3%	2.4%	2.2%	2.4%
		Models					
		ln1 model	ln2 model	ln3 model	Sn1 model	Sn2 model	Sn3 model
C_{TL}	FEM (0~350 Hz)	902.17	575.1	334.83	244.51	575.1	1130.4
	Eq.(12)	958.63	603.58	346.74	242.43	603.58	1202.2
	Relative error	5.9%	4.7%	3.4%	0.9%	4.7%	6%
	FEM (0~1000 Hz)	935.89	590.2	340.32	248.36	590.2	1185.3
	Eq.(12)	958.63	603.58	346.74	242.43	603.58	1202.2
	Relative error	2.4%	2.2%	1.9%	2.4%	2.2%	1.4%

4. Conclusion

This paper presents a theoretical analysis of the noise attenuation capacity C_{TL} and first proposes the theoretical formula of C_{TL} . The C_{TL} is defined as the integral of transmission loss in the frequency domain. The effects of the neck length, cross-sectional area of the neck, cavity volume and cross-sectional area of the duct on C_{TL} are analyzed theoretically and numerically. The C_{TL} calculated by the proposed theoretical formula shows a good agreement with the FEM simulation result among all the models. The results indicate that the C_{TL} is only related to the geometries of the neck and the cross-sectional area of the duct. The cavity volume has no effects on the C_{TL} . Similar to the significance of the HR's resonance frequency, the proposed theoretical formula of C_{TL} should therefore be considered as one of the main acoustic characteristics of the HR. It provides a distinct parameter to evaluate the HR's noise attenuation band quantitatively and

illuminates the limitations in HR's noise control applications. The C_{TL} is an important supplement to the theoretical studies and engineering applications of HRs. It is hoped that the present study could provide a stepping stone for the investigation of the HR's or other silencers' noise attenuation capacity and potential applications in all research areas in respect of the HR.

Acknowledgements

The work described in this paper was fully supported by a grant from the Research Grants Council of the Hong Kong Special Administrative Region, China (Project No. PolyU 152116/14E).

References

[1] Munjal ML. Acoustics of Ducts and Mufflers. New York: Wiley, 1987.

[2] Bies DA, Hansen CH. Engineering noise control: theory and practice. 4th ed. London: Spon Press; 2009.

[3] Mak CM, Yang J. A prediction method for aerodynamic sound produced by closely space element in air ducts. J Sound Vib 2000;229(3):743-753.

[4] Cai C, Mak CM, Wang X. Noise attenuation performance improvement by adding Helmholtz resonators on the periodic ducted Helmholtz resonator system. Appl Acoust 2017;122:8-15.

[5] Isozaki A, Takahashi H, Tamura H, Takahata T, Matsumoto K, Shimoyama I. Parallel Helmholtz resonators for a planar acoustic notch filter. Appl Phys Lett 2014;105:241907.

[6] Ma G, Sheng P. Acoustic metamaterials: From local resonances to broad horizons. Sci Adv 2016;2:e1501595.

[7] Monkewitz PA, Nguyen-Vo NM. The response of Helmholtz resonators to external excitation. Part 1. Single resonators. J Fluid Mech 1985;151:477-497.

[8] Selamet A, Dickey NS. Theoretical, computational and experimental investigation of Helmholtz resonators with fixed volume: lumped versus distributed analysis. J Sound Vib 1995;187(2):358-367.

[9] Selamet A, Ji ZL. Circular asymmetric Helmholtz resonators. J Acoust Soc Am 2000;107(5):2360-2369.

[10] Li L, Liu Y, Zhang F, Sun Z. Several explanations on the theoretical formula of Helmholtz resonator. Adv Eng Softw, published online.

[11] Cai C, Mak CM, Shi X. An extended neck versus a spiral neck of the Helmholtz resonator. Appl Acoust 2017;115:74-80.

[12] Cai C, Mak CM. Acoustic performance of different Helmholtz resonator array configurations. Appl Acoust 2018;130:204-209.

[13] Zhao D. Transmission loss analysis of a parallel-coupled Helmholtz resonator network. AIAA J 2012;50(6):1339-1346.

[14] Li J, Wang W, Xie Y, Popa B, Cummer SA. A sound absorbing metasurface with coupled resonators. App Phys Lett 2016;109;091908.

[15] Li Y, Assouar BM. Acoustic metasurface-based perfect absorber with deep subwavelength thickness. App Phys Lett 2016;108;063502.

[16] Park SH. Acoustic properties of micro-perforated panel absorbers backed by Helmholtz resonators for the improvement of low-frequency sound absorption. J Sound Vib 2013;332:4895-4911.

[17] COMSOL, COMSOL Multiphysics Reference Guide, version 5.1; 2015.

[18] Kergomard J, Garcia A. Simple discontinuities in acoustic waveguides at low frequencies: Critical analysis and formulae. J Sound Vib 1987;114:465-479.

Figure captions

Fig.1 Mechanical analogy of a Helmholtz resonator

Fig. 2 The acoustic FEM models of side-branch HRs with respect to different HRs: (a) HR1 model, (b) HR2 model, (c) HR3 model

Fig. 3 Comparison of theoretical predictions and the FEM simulation results with respect to different HRs (solid lines represent the theoretical predictions, and dashed crosses represent the FEM simulation results)

Fig. 4 Normalized transmission loss of different HRs

Fig. 5 The acoustic FEM models of the identical HR mounted on different ducts with respect to different cross-sectional areas: (a) Sd1 model, (b) Sd2 model, (c) Sd3 model

Fig. 6 The transmission loss of the identical HR mounted on ducts with different cross-sectional areas (solid lines represent the theoretical predictions, and dashed crosses represent the FEM simulation results)

Fig. 7 The acoustic FEM models of side-branch HRs in respect of different neck geometries: (a) ln1 model, (b) ln2 model, (c) ln3 model, (d) Sn1 model, (e) Sn2 model, (f) Sn3 model

Fig. 8 Comparison of theoretical predictions and the FEM simulation results with respect to different HRs (solid lines represent the theoretical predictions, and dashed crosses represent the FEM simulation results)

Fig. 9 Normalized transmission loss of different HRs

Table captions

Table 1. Relative error between the FEM simulation result and value of Eq. (12)